Fabrication of Carbon Nanotube Networks on Three-Dimensional Building Blocks and Their Applications

20121027

Name of Principal Investigator : Haiwon Lee

- e-mail address : haiwon@hanyang.ac.kr
- Institution : Hanyang University
- Mailing address : Department of Chemistry, Hanyang University, 17 Haengdang-dong, Seongdong-gu, Seoul 133-791, Korea
- Phone: +82-2-2220-0945
- Fax: +82-2-2296-0287

Period of Performance: 06/13/2011 – 06/27/2012

Report Documentation Page

Form Approved
OMB No. 0704-0188

1. REPORT DATE	2. REPORT TYPE	3. DATES COVERED
27 OCT 2012	**Final**	**13-03-2011 to 27-06-2012**

4. TITLE AND SUBTITLE
Fabrication of Carbon Nanotube Networks on Three-Dimensional Building Blocks and Their Applications

5a. CONTRACT NUMBER
FA23861114016

5b. GRANT NUMBER

5c. PROGRAM ELEMENT NUMBER

6. AUTHOR(S)
Haiwon Lee

5d. PROJECT NUMBER

5e. TASK NUMBER

5f. WORK UNIT NUMBER

7. PERFORMING ORGANIZATION NAME(S) AND ADDRESS(ES)
Hanyang University,Department of Chemistry,Haengdang-dong, Seongdong-gu,Seoul ,KR,133-791

8. PERFORMING ORGANIZATION REPORT NUMBER
N/A

9. SPONSORING/MONITORING AGENCY NAME(S) AND ADDRESS(ES)
AOARD, UNIT 45002, APO, AP, 96338-5002

10. SPONSOR/MONITOR'S ACRONYM(S)
AOARD

11. SPONSOR/MONITOR'S REPORT NUMBER(S)
AOARD-114016

12. DISTRIBUTION/AVAILABILITY STATEMENT
Approved for public release; distribution unlimited

13. SUPPLEMENTARY NOTES

14. ABSTRACT

Three-dimensional (3D) networks of carbon nanotubes (CNTs) were fabricated on a pillar- patterned substrate by plasma-enhanced chemical vapor deposition (PECVD). To fabricate 3D networks of CNTs, highly crystalline single-walled CNTs (SWCNTs) should be synthesize on the substrate. PECVD has advantages for low temperature growth and alignment of CNTs on the substrate, but it is difficult to synthesize highly crystalline SWCNTs using this technique due to the plasma etching effect. To reduce the plasma etching effect, a metal mesh was installed above the substrate. The use of the mesh allowed the fabrication and modification of highly crystalline SWCNT 3D networks minimizing the plasma etching effects.

15. SUBJECT TERMS

16. SECURITY CLASSIFICATION OF:			17. LIMITATION OF ABSTRACT	18. NUMBER OF PAGES	19a. NAME OF RESPONSIBLE PERSON
a. REPORT	b. ABSTRACT	c. THIS PAGE			
unclassified	**unclassified**	**unclassified**	**Same as Report (SAR)**	**28**	

1.Fabrication of highly crystalline carbon nanotube networks and surface modification in a Si-pillar substrate

Abstract

Three-dimensional (3D) networks of carbon nanotubes (CNTs) were fabricated on a pillar-patterned substrate by plasma-enhanced chemical vapor deposition (PECVD). To fabricate 3D networks of CNTs, highly crystalline single-walled CNTs (SWCNTs) should be synthesize on the substrate. PECVD has advantages for low temperature growth and alignment of CNTs on the substrate, but it is difficult to synthesize highly crystalline SWCNTs using this technique due to the plasma etching effect. To reduce the plasma etching effect, a metal mesh was installed above the substrate. The use of the mesh allowed the fabrication and modification of highly crystalline SWCNT 3D networks minimizing the plasma etching effects.

Introduction

Carbon nanotubes (CNTs) have attracted much attention for promising application such as field effect transistor, energy device and sensor due to their chemical, physical and electrical properties. In order to apply these properties to devices, synthesis and manipulation of isolated CNTs on a template are important. In recent years, the improvement of device performance using a high density CNTs array has become the focus of research. However, in terms of manipulation methods, it is difficult to allocate CNTs in the three-dimensional (3D) structures. Direct syntheses of suspended CNTs on 3D templates have been reported, and then 3D structure of suspended CNTs became an emerging issue to expand potential applications beyond the limit of two dimensional (2D) devices. Up to the present, most researches on suspended CNTs were conducted by using SWCNTs because multi-walled CNTs (MWCNTs) are unlikely flexible enough for the fluctuation of directional growth. Moreover, so far, suspended SWCNTs have been accomplished by using thermal CVD only. However, this growth method did not yield suspended SWCNTs but suspended MWCNTs, and had a limitation that requires a special (short/float) electrode pair to form the lateral electric field for unidirectional growth of MWCNTs. And plasma induced by electric field is unlikely to fabricate defect free and isolated SWCNTs, because plasma etching effect, which is reported to damages CNTs, is proportional to electric field energy. In this study, we report the first successful synthesis of 3D networks of SWCNTs on the pillar substrate and the surface modification of SWCNT by using mesh-installed PECVD without any accompanying electrode. The metal mesh was installed above the substrate to decrease the plasma etching effect on horizontal growth of SWCNT in between pillars.

Experiment

Preparation of catalyst-deposited pillar substrate: A micro- sized pillar structure was fabricated on Si (100) substrate using a photolithography and a deep Si etching process. The Si-pillar substrate, which has a 3 μm height, 1 μm diameter and distance Si-pillars, was immersed in piranha solution (7:3 mixture of H_2SO_4 and H_2O_2) to remove organic contaminants and to modify the surface with hydroxyl group, and then rinsed with de-ionized water to remove the piranha solution from the surface of pillar substrate. In order to deposit catalyst on the entire surface of the pillars, the substrate was soaked in Fe-Mo organo- metallic complex solution. The Fe-Mo solution was prepared by $Fe(NO_3)_3 \cdot 9H_2O$ (Junsei) and Mo solution (ICP/DCP standard solution, Aldrich) with ultrasonication for 20min in ethanol.

Synthesis of CNTs by mesh-installed PECVD: The CNTs were synthesized on the catalyst-deposited substrate in the chamber of mesh-installed PECVD (ICP-CVD, A-tech system) at an inductively coupled radio frequency (13.56 MHz). The mesh was made of stainless steel and had a large number of 2 mm diameter holes with 1 mm spacing. The position of installed mesh was adjusted to 10 mm apart from the substrate. For the synthesis of CNTs, the chamber was pumped down to less than 1.0 X 10^{-6} torr. While hydrogen (H_2) gas plasma (100 W, 0.05 torr, and 50 sccm) was maintained for 15 min, the substrate was heated from 30 ℃ to 750 ℃. When the temperature of substrate was saturated at 750 ℃, acetylene (C_2H_2) gas was introduced additionally into the chamber to synthesize CNTs for 1 min (50W, 0.05 torr and 15 sccm). After synthesis of CNTs, the chamber was cooled down to the room temperature. In order to incorporate amino groups on the 3D network of CNTs, NH_3 RF plasma was carried out in the mesh-installed PECVD chamber at 50 W, 0.05 torr and 25℃ for 10 min.

Characterization: The structure and the morphology of CNTs grown on the pillar substrate were characterized with a scanning electron microscope (SEM, S-4700, Hitachi) and a transmission electron microscope (TEM, TECNAI-F20, 200 keV, Philips). Raman spectroscopy (NRS-3000, 514 nm laser excitation wavelength, Jobin-Yvon) was used to characterize the crystallinity of the as-synthesized CNTs. In addition, Atomic force microscope (AFM, XE-100, PSIA) was used to confirm the size of the catalyst nanoparticles that were formed on the substrates.

Results and Discussion: SEM images of the CNTs synthesized on the pillar substrate by PECVD with the mesh- installed are shown in Figure. 1a-b. Most of the CNTs were grown from the sidewalls of the pillars in a random direction and formed networks with the nearest adjacent pillars. Due to this 3D network formation, the total surface area of CNTs was increased compared to the 2D structure of CNTs based on the number of interconnections. When CNTs form a 3D network in between pillars, they are agglomerated by the van der Waals forces and thermal vibration of each CNT. In case of the conventional PECVD process without a mesh, CNTs are entangled around the pillars instead of networking between pillars as shown in

Figure 1c-d. The interconnected CNTs were composed of SWCNTs in both individual and bundle structure, as shown in the TEM image of figure 2. The Raman spectra of the SWCNTs revealed several radial breathing mode (RBM) peaks between 100 and 350cm^{-1} (Figure. 3a). The diameter of most of the SWCNTs was 0.8 to 1.5 nm, which was confirmed by RBM frequency as well as the TEM image. In the Raman spectrum, the intensity ratio of the D-band (~1350 cm^{-1}) to the G-band (~1590 cm^{-1}) (I_D/I_G) could be correlated with the crystallinity and the purity of CNTs. The Raman spectrum of figure 3a showed a low I_D/I_G ratio (~0.24), which may suggest that highly crystalline SWCNTs have been synthesized on the pillar substrate by the mesh-installed PECVD. However, the conventional PECVD without mesh created the entangled CNTs, which were induced by many defects. The high I_D/I_G ratio (~1.31) in Raman spectrum (Figure. 3b) indicates that entangled CNTs have large quantities of defects caused by the bombardment of the accelerated ions. When the ion bombardment takes place during CNT growth, C-C bonds breaking, called the plasma etching effect, competes with the formation of the C-C bond on the catalyst surface. The ion bombardment also affected the generation of defects on the surface of CNTs.

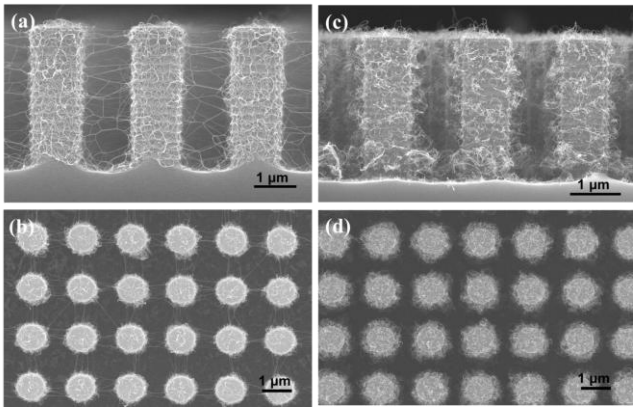

Figure 1. SEM images of CNT grown on the pillar patterned substrate by (a-b) mesh-installed PECVD and (c-d) conventional PECVD.

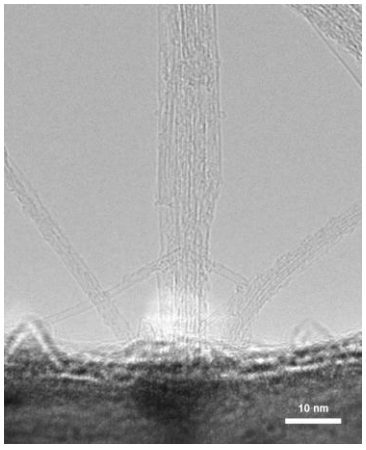

Figure 2. A TEM image of the bundles of SWCNTs fabricated by mesh-installed PECVD.

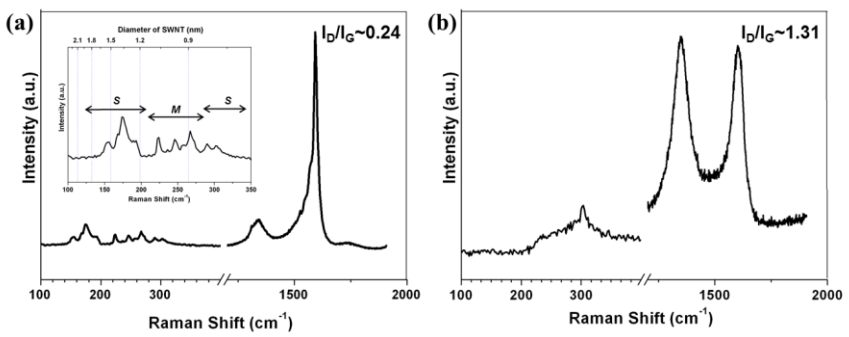

Figure 3. Raman spectra of (a) the network-structured CNTs fabricated by mesh-installed PECVD and (b) the entangled CNTs fabricated by conventional PECVD.

To synthesize the 3D network of CNTs on the pillar substrate by PECVD, two conditions should be satisfied. One is minimizing the plasma etching effect for the synthesis of high crystalline CNT and the other is synthesis of SWCNTs on the surface of pillars. The plasma etching effect is dependent on the ion bombardment energy (E_i), which is influenced by input power (W) and ions flux (J_i). The relation of E_i, J_i and W is in the forms of $E_i \propto J_i$ and $J_i \propto W$. Thus, the ion bombardment energy and ion flux can be decreased by lowering the input power. However, for the synthesis of the high density CNTs, the magnitude of J_i should be maintained at a sufficient high level. The J_i is expressed by $J_i \propto \rho v_i$, where ρ is the density of ions in unit area and v_i is velocity of ion. Therefore, ρ should be maintained at sufficient level while depressing the v_i for minimizing plasma etching effect.

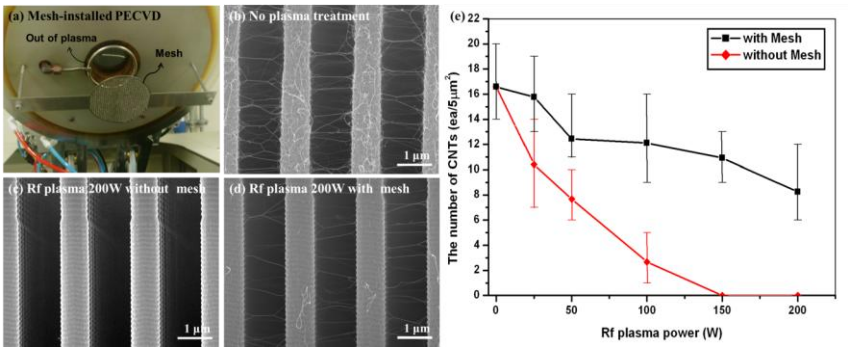

Figure 4. (a) A mesh was installed under the plasma apparatus in PECVD. (b-d) SEM images of comparing plasma etching effect on the CNTs 3D network structure and (e) the density variation of CNTs in the function of RF plasma power.

In order to reduce the plasma etching effect, a mesh was installed under the plasma apparatus, as shown in Figure. 4a. Ions generated from the plasma could freely diffuse through the holes in the mesh, but lose their kinetic in doing so. Figure 4b-d shows the SEM images of the effects of metal mesh against the plasma etching effect at 750℃ for 20 min under H_2 gas plasma with an

RF power of 200 W. Before the H_2 plasma treatment, as-synthesized SWCNTs were interconnected between pillars, forming networks as shown in Figure. 4b. When the SWCNTs network was exposed to H_2 plasma, all the SWCNTs were disconnected (Figure. 4c). In contrast, after plasma treatment with a mesh, the greater part of SWCNTs network still remained (Figure. 4d). The numbers of interconnected CNTs versus plasma power with and without the mesh are plotted in Figure 4e. The number of interconnected CNTs without the mesh was significantly decreased with the increase in the plasma power. This difference in the SWCNTs etching with and without the mesh indicates that the installed mesh effectively reduces the ion bombardment effect by lowering the kinetic energy of ions and lowering the ion flux. Figure 5 shows the I_D/I_G ratio of the Raman spectra with and without the plasma treatment. The I_D/I_G of sample by mesh-installed PECVD was almost comparable to that of the non-plasma-treated sample. However, the I_D/I_G ratio definitely decreased without the mesh installation. As a result, it is verified that the mesh played an important role to reduce the plasma etching effects on CNTs.

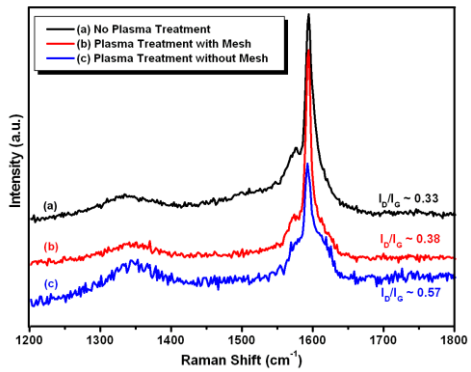

Figure 5. Raman spectra of the 3D network of CNTs before and after plasma treatment with/without mesh.

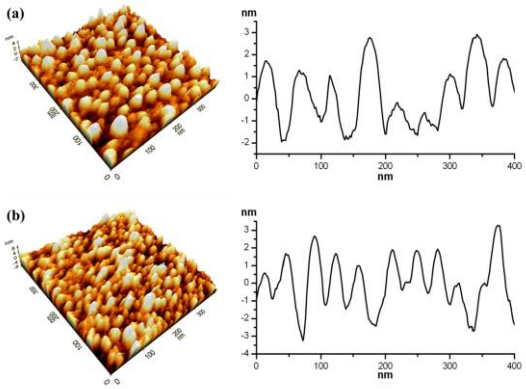

Figure 6. AFM topographic images of catalyst nanoparticles formed on the Si substrate by (a) the conventional process and (b) the heating-pretreatment-combined process.

In general, when CNTs are synthesized in CVD, the number of CNT walls is affected by the catalyst particle size. For the synthesis of SWCNTs, the size of the catalyst particle should be decreased by adjusting the process conditions such as temperature, pretreatment and catalyst layer thickness. To reduce the catalyst particle size, a combination of heating and pretreatment processes was carried out instead of using a conventional pretreatment process which is treated after the heating process. The direct imaging of catalyst nanoparticles on the sidewall of pillar is unrealizable. For evaluation of catalyst particles, instead of it, catalyst was deposited on the planar Si substrate under the same conditions and the topographic images of the catalyst nanoparticles after different pretreatments evaluated by AFM as shown in Figure. 6. In the case of the conventional method, where the processing condition is thermal heating to 750 ℃ for 10 min and subsequent H_2 plasma pretreatment for 5 min, the average diameter of the catalyst particles was 27.6 nm on the Si substrate (Figure 6a). In the combined process, heating was carried out from 30℃ to 750℃ for 15 min under hydrogen (H_2) gas plasma pretreatment. Figure 6b shows that the size of the catalyst nanoparticles decreased compared with the size of catalyst particle prepared using the conventional method. The average diameter of the catalyst particles was 18.4 nm. It should be noted that the surface morphology of pillar sidewall is different from the planar Si substrate. So, the different size of catalyst particles could be formed. Nevertheless, figure 6 suggests that H_2 plasma treatment in combined process is effective in decreasing the size of the catalyst particles because the iron oxide atoms were more effectively evaporated and reduced on the substrate under H_2 treatment. The reduction process of iron oxide follows these reactions:

$$3Fe_2O_3 + H_2 \rightarrow 2Fe_3O_4 + H_2O \qquad (1)$$

$$3Fe_3O_4 + 4H_2 \rightarrow 3Fe + 4H_2O \qquad (2)$$

Due to the decrease of catalyst size, SWCNT could be synthesized on the Si-pillar substrate and forms a network structure.

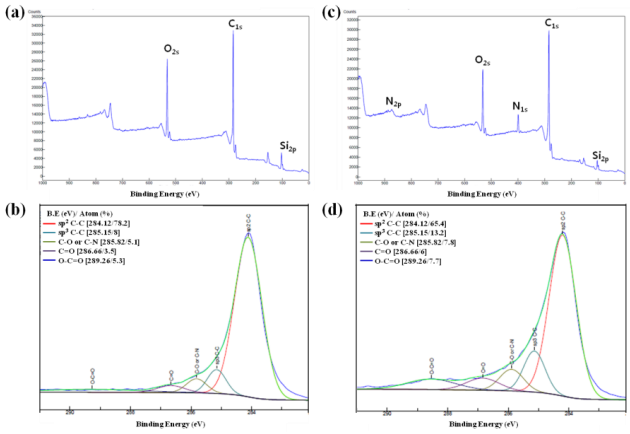

Figure 7. XPS spectra of (a-b) as-synthesized SWNTs and (c-d) after NH_3 plasma treatment.

In order to confirm surface modification of SWNT using RF plasma, XPS analysis was carried out. Figure 7 shows XPS spectra of SWNT treated by NH_3 plasma. These spectra show presence of carbon, nitrogen and oxygen. Especially, Figure 7c shows that surface of SWNT is expected to included nitrogen containing functional group (amino, amide, amine, etc.) after NH_3 plasma treatment compared with Figure 7a. It can be also confirmed at high resolution C_{1s} spectrum of Figure 7d, which nitrogen concentration is increased compared to pristine SWNT XPS spectrum as shown in Figure 7b. Also, the quantitative analysis indicated slightly increased from 5.1 % to 7.8 % after NH_3 plasma treated.

Conclusion: A SWCNT network was fabricated on between Si-pillars using PECVD with a mesh-installed above the substrate. Both the reduction of the plasma etching effects and the formation of small catalyst particles are important factors for the formation of SWCNTs network. The utilization of a mesh above the substrate was effective to suppress the plasma etching effect, resulting in successful interconnection of SWCNTs. The SWCNTs network was well formed and maintained between the neighboring pillars under the mesh during the growth process. Also, additional NH_3 plasma treatment with mesh is effective to modify surface of SWCNTs structure to nitrogen containing functional group. After plasma treatment, the surface defect of SWNT slightly increased, but the network structure is not damaged. Plasma treatment with mesh is an effective method for modification of SWCNT 3D network structure. The 3D network of SWCNTs containing various functional groups is expected to increase the sensitivity in sensor devices as a result of their large surface area.

2. Hierarchical and Multifunctional Three-dimensional Network of Carbon Nanotubes for Microfluidic Application.

Abstract

The 3D network of CNTs has hierarchical structures comprised of interconnected SWNTs between Si pillars in microfluidic channels. The Al_2O_3 coated 3D networks were used for size different nanoparticles filtration and streptavidin capturing in diluted solution. The 3D network of SWNTs systems will provide a robust multifuncitonal platform for a variety of biomedical and environmental applications.

Introduction

Filtration and capture in microfluidic systems are becoming increasingly important in a variety of biomedical and environmental, applications. The on-chip filtration is able to handle small amounts of liquid and analyte, and also it increases the detection efficiency via sorting of analyte. There are some reports for sorting or separating blood cell, colloidal and bacteria by using channels which were fabricated on a silicon and glass wafer. Recently, three-dimensional(3D) hierarchiral structures consisting of micro- and nanofabricated pillars have been introduced as effective structures. These systems allow for considerable increases in the contact area between substrates and target materials, thus enhancing the filtration and capture efficiency of nanoparticles and chemical materials.

Carbon nanotubes (CNTs) have excellent mechanical, electrical and chemical properties for a variety of applications. Especially, arrays of CNTs on 2D or 3D substrates are advantageous over the systems based on individual CNTs. Homma et al. and Hong et al. reported the growth of suspended single-walled CNTs(SWNTs) networks on the tops of micro- and nanofabricated Si pillars, and Lu et al. reported the synthesis of 3D suspended SWNTs on sloped silicon surface. We recently reported the synthesis of suspended 3D network of SWNTs inside the porous Si substrate using a dipping method. This approach enables uniform adsorption of catalyst nanoparticles onto the whole surface area of complex structures.

Some of groups studied the use of CNTs for filtration and separation applications. These were effective in removing small amount of virus, oil and low molecules solute. However such filters require high pressure for operation. Although CNT has high surface area that is good for using capture materials, densely packed structure of CNTs tend to pore plugging and performance deterioration upon filtration of environmental samples. And the structure couldn’t filter by size of materials.

In this work, we leveraged these 3D CNT structures to develop a new type of microfluidic platform. The 3D network of CNTs has hierarchical structures comprised of interconnected SWNTs between Si pillars in microfluidic channels. The 3D network of CNTs was coaxially coated with Al_2O_3 by atomic layer deposition (ALD) to prevent CNTs from aggregation in microfluidic chips. The Al_2O_3 coated 3D networks were used for nanoparticles filtration and streptavidin capturing.

Experiment

Preparation of Si pillar arrays: The Si pillar array (Figure. 1) was fabricated on a highly doped n-type Si (100) substrate by using a general photolithography technique which included a deep Si etching process (SLR-770-10R-B, Plasma Thermo Co.). In order to clean and modify the surface of Si pillar array with hydroxyl groups, the substrate was socked in a piranha solution (H_2SO_4: H_2O_2 = 3 : 1) for 1 hours. The Si pillar substrate was then washed by de-ionized (DI) water to remove the piranha solution from the substrate.

Formation of catalyst on Si pillar surface: A catalyst solution was prepared by ultrasonication using $Fe(NO_3)_3 \bullet 9H_2O$ (Junsei), Mo solution (ICP/DCP standard solution, Aldrich), and an ethanol solvent. The molar ratio of Fe/Mo in the catalyst solution was 7/1. To form the Fe-Mo catalyst nanoparticles on the Si pillar arrays, the substrate was soaked in the Fe-Mo catalyst solution for 60 minutes, and then fully rinsed with ethanol. As a result, Fe-Mo catalyst nanoparticles were uniformly formed on the entire surface area of the Si pillar arrays.

Synthesis of CNTs: The CNTs was synthesized in a horizontal quartz tube reactor using low pressure thermal chemical vapor deposition (LPTCVD). The diameter and the length of the reactor are 40 and 800 mm, respectively. The substrate was inserted into the center of the reactor. After the thermal annealing at 400°C for 30 min in air at ambient pressure, the reactor was pumped down to a pressure lower than ~ 9.0×10^{-3} torr and heated up to 800°C. When the temperature of the reactor reached 800°C, 300 sccm of NH_3 gas was introduced into the reactor for 10 min to reduce the iron oxide to the iron catalyst. After the NH_3 pretreatment, 10 sccm of C_2H_2 gas was introduced for 20 min to synthesize CNTs while maintaining a pressure of 3.3×10^{-1} torr. Finally, the reactor was cooled down to room temperature under a pressure of 9.0×10^{-3} torr.

Characterization of CNTs: A scanning electron microscope (SEM, S-4800, Hitachi), a transmission electron microscope (TEM, JEM 2100-F, 200 keV, Jeol), Raman spectroscopy (LabRam HR, 514 nm laser excitation wavelength, Jobin-Yvon)

Atomic Layer Deposition with Al_2O_3: The atomic layer deposition (ALD, Cyclic 4000, Genitech) was introduced to deposit the Al_2O_3 on the surfaces of network-structured CNTs with $Al(CH_3)_3$ (Aldrich, 99%) and H_2O as precursors. Ar gas with a flow rate of 50 sccm was supplied for carrying and purging of the precursors. The cycles of exposure were programmed as 1 sec for trimethyl aluminum (TMA), 5 sec for Ar, 1 sec for H_2O, and 5 sec for Ar. The Al_2O_3 was grown as thin film with a temperatures range of 150 to 200 °C and a pressure of 300 m torr.

Fabrication of Microfluidic Filtration and Characterization: The microchannel was simultaneously fabricated with the same process as silicon pillar patterns on the silicon substrate.

The network-structured CNTs were grown in the filtration region which was positioned at the channel center with pillar patterns. Then, the microchannel was bonded with a PDMA cover and connected to syringe pumps (Pump 11 Pico Plus, Harvard Apparatus). An ethanol solution dispersed with aqueous fluorescent polystyrene particles (G500, Duke Scientific Corporation) was injected into the inlet. The fluorescent images were obtained by fluorescence microscope (BX51, Olympus) with a CCD camera (DP70, Olympus).

Substrate silanization: The Al_2O_3 coated 3D SWNT substrates were rinsed with chloroform and set in a UV–ozone cleaner (Irvine, CA) for 3 h prior to silanization. *N*-(2-aminoethyl)-3-aminopropyltrimethoxysilane (AEAPS) was purchased from Gelest, Inc. (Tullytown, PA). Freshly cleaned substrates were silanized in a 1% AEAPS solution in methanol (95% methanol, HPLC grade, Sigma Aldrich) for 1.5 h at room temperature. The substrates then were rinsed three times with methanol and blown dry with purified N_2.

Biotin modified and streptavidin capture : The AEAPS modified substrate was covered for 1 h with phosphate-buffered saline (PBS; pH 7.4) containing biotin(5 mg/mL). After the reaction, the substrate was rinsed to remove unbound biotin. Then, the microchannel was bonded with a PDMA cover and connected to syringe pumps. And it was injected with 1 mL of PBS containing streptavidin(300 ng/mL) and flowed with PBS buffer. The fluorescent images were obtained by same the same fluorescence microscope.

Results and Discussion

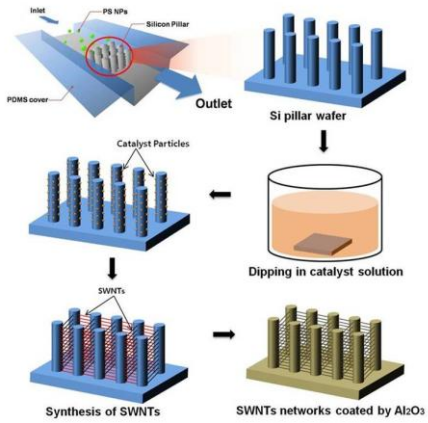

Scheme 1. Schematic illustrations of the procedures for the fabricating 3D network of SWNTs on Si pillar template.

Scheme 1 shows the experimental procedure for fabricating 3D network of CNTs on a Si pillar template in a microfluidic chip. The microfluidic template was fabricated on a Si substrate using a photolithographic technique. For the adsorption of Fe-Mo bicatalyst nanoparticles on Si pillar

templates, the substrate was soaked in the catalyst solution for few minutes followed by ethanol rinsing. The SWNTs were synthesized by thermal chemical vapor deposition.

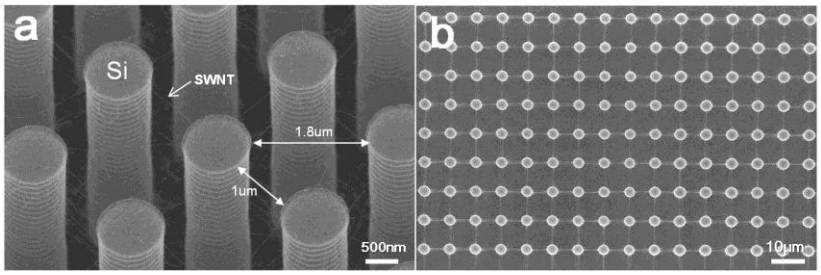

Figure 1. SEM images of 3D network of SWNTs synthesized between the Si pillar template : (a) tilted view with 30°, (b) top view.

Figure 1 shows entire interconnection of suspended SWNTs networks between Si pillars. The diameter and height of the as-prepared Si pillars were 1.0 and 28.0 μm, respectively. The small and large gaps between two adjacent Si pillars were 1.0 and 1.8 μm, respectively. The interconnected SWNTs between adjacent pillars are straight as reported previously. Most of the suspended SWNTs were formed between adjacent Si pillars with a small gap, and a few of them were formed between two Si pillars seperated by a large gap. As the gap of adjacent pillars increases, the number of interconnected SWNTs decreases and also the gap between adjacent SWNTs increases. The directional formation of SWNTs between adjacent Si pillars has been reported as a combination of the geometrical effect of the pillar structure and the thermal vibration effect from the SWNTs. It showed that the SWNTs formed a 3D network structure, not only through the Si pillar array, but also through connections with each other in 3D space. This arrangement is due to the overgrowth of SWNTs and the van der Waals interactions between them. This result implies that the catalyst nanoparticles were formed over the entire surface area of the dense Si pillar array by the dipping method. The SWNTs were confirmed by Raman spectra. Raman analysis with a micro sized laser-beam was conducted at three different vertical positions between two adjacent Si pillars, as indicated in Figure 2. Figure 3 shows that clear peaks in the radial breathing mode(RBM) frequency appeared in all spectra. These Raman results indicate that the SWNTs were synthesized over the entire vertical area between the adjacent Si pillars, but that the mean diameter of the SWNTs located at the bottom of the pillar structures was larger than that of the SWNTs located at the top of the pillar structures. This difference implies that the sizes of iron nanoparticles are different slightly depending on their vertical positions within the pillar structure. This phenomenon may be due to the difference in catalyst removal from long, dense Si pillar structure during the dipping process. TEM analysis revealed that the SWNTs have bundle structures because of interconnection for bundling in 3D space, which corresponds with the data in the SEM image. The 3D network of CNTs were aggregated after dipping and drying from solution. When the substrate of 3D network of SWNTs was dipped

into either hydrophilic or hydrophobic solution such as water, hexane, acetone and toluene, all CNT networks were aggregated.

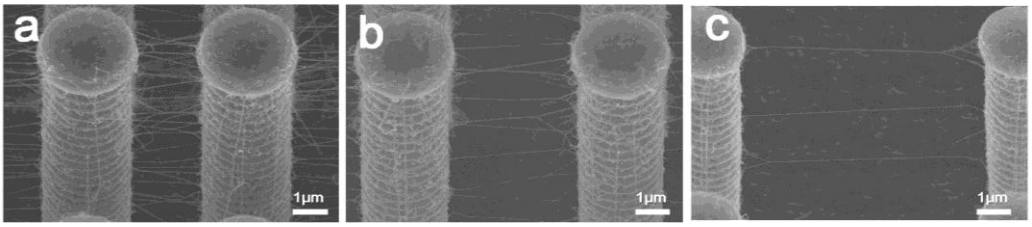

Figure 2. SEM images of 3D network of SWNTs synthesized between the Si pillars template: each gap between pillars is (a) 2.5 μm, (b) 5 μm and (c) 10 μm

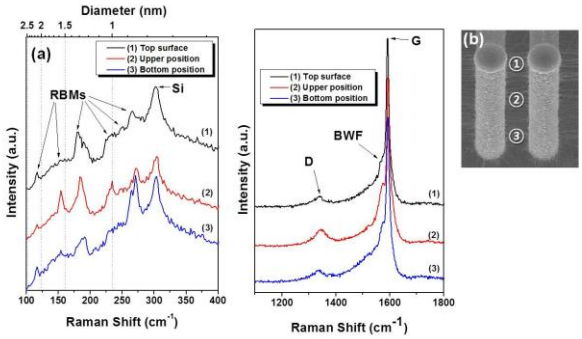

Figure 3. (a) Raman spectra of 3D network of SWNTs synthesized on different vertical areas of two adjacent Si pillars. The laser excitation wavelength was 514 nm. (b) SEM image of 3D network of SWNTs. The circled numbers indicate the measurement points of the raman analysis.

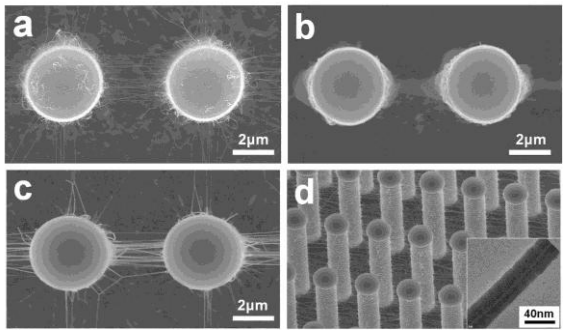

Figure 4. SEM images of (a) as-grown 3D network of SWNTs, (b) destructed network structured SWNTs without Al_2O_3 coating by a microchannel flow, (c) sustained network-structured SWNTs with Al_2O_3 coating after a microchannel flow test and (d) Al_2O_3 coated 3D network of SWNTs(low magnified image) and TEM micrograph reveals the 15nm coating to be uniform and continuous(inset).

The as-grown 3D network of SWNTs has this problem, so the surface modification of CNT is necessary for use in microfluidic chips. Figure 4a and 4b show that the network structures of as-grown CNTs were collapsed under fluid flow. This is presumably because the adhesion force

between CNTs is larger than the binding force between CNTs and pillars, failing to preserve the original CNT networks. Figure 4c shows the SEM images of 3D network of SWNTs after Al_2O_3 coating by ALD, and both CNTs and pillars were uniformly coated. In the TEM image in Figure 4d, the thickness of the Al_2O_3 layer was 15 nm. After coating the template by ALD, the network structures were well sustained under liquid flow in a fluidic channel. By ALD, the surface properties of 3D networks were changed, and thus the coated network structures could be used for filtration and chemical modification.

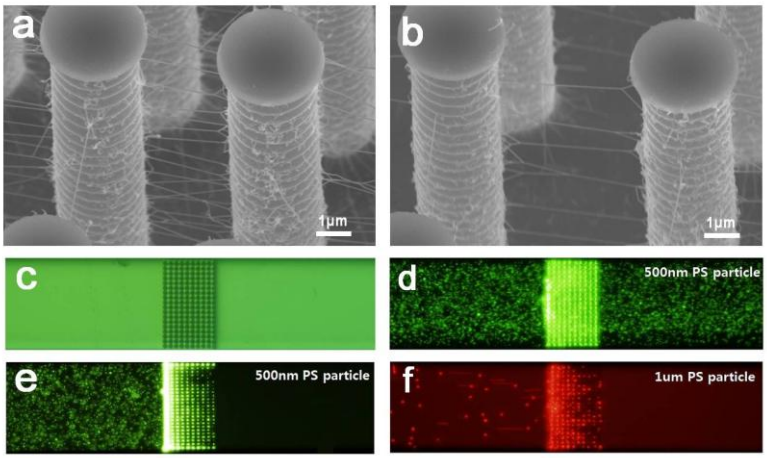

Figure 5. SEM images and optical images of Al_2O_3 coated 3D network of SWNTs on (a, c, e) 2.5μm spacing and (b, d, f) 5 μm spacing Si pillar templates in microfluidic channel. (c) Microscopic image of Si micropillar in microfluidic channel. And fluorescent microscopic images of (d) passing 500 nm green-PS particles through 3D networks on 5 μm spacing Si pillar template, (e) filtered 500 nm green-PS particles by 3D networks on 2.5 μm spacing template, and (f) filtered 1μm red-PS particles by 3D networks on 5μm spacing template.

Figure 5 shows that the network structures with different gaps are able to filter the different size particles. For filtration, the microchannel was bonded to a PDMS cover and connected to syringe pumps. An ethanol solution dispersed with aqueous fluorescent polystyrene particles with 500 nm in diameter was injected into the inlet at a flow rate of 0.02 μL/min (average flow velocity was 40 μm/s). Figure 5c-f show the images of 3D networks in microfluidic channels. When a fluid flow was generated through the microchannel, the fluorescent polystyrene (PS) nanoparticles completely pass through the pillar region of non-CNT networks. However, the nanoparticles were well filtered by the 3D networks in the pillar region. Figure 5e shows that green fluorescent 500 nm diameter particles were filtered by CNT network structures formed between pillars of 2.5 μm gap. In case of 5 μm spaced pillar template, the 500 nm particles completely passed through the Al_2O_3 coated 3D network of CNTs. In Figure 5f, 1 μm red-colored PS particle were filtered by the CNT network structures on 5 μm gap pillar template. In this system, the solution was flowed by only capillary force, so that the 3D networks filtration system is especially useful for sorting the soft materials in mild condition.

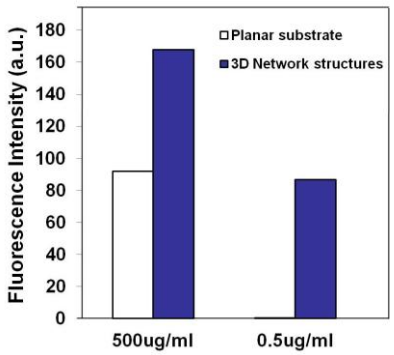

Figure 6. Fluorescence intensity comparison of the streptavidin captured on the biotin immobilized 3D network structures and planar substrate in microfluidic channel.

For the extension of this approach to biomaterial assays, the networks coated with Al_2O_3 were silanized to functionalize with biotin. No difference between biotin modified substrate and non-treated substrate was observed by optical microscope image. The biotin-modified 3D networks gave off the green fluorescence after flowing the green-dye tagged streptavidin solution which has a concentration of 300 ng/ml. The optical image shows only top image of Si pillars after flowing of streptavidin. Furthermore, the fluorescence intensity was measured by changing streptavidin concentration, and the result from 3D network structures was compared with the result from a planar substrate which was fabricated without Si pillars in microfluidic chip. However, no significant increase of fluorescence intensity at above the concentration of 500μg/ml was observed because of the signal saturation as reported in elsewhere. Figure 6 shows that the difference of fluorescence intensity is about 2 times in high concentration solution. However, in 1000 times diluted solution, the intensity difference is about 190 times. These results demonstrate the potential of system for the development of novel fluorecence-based chemical sensors and biosensors.

Conclusion : In summary, a new type of microfluidic template based on the 3D network of SWNTs on Si pillar substrate was fabricated to do efficient filtration with high selectively. And the template was able to capture streptavidin. Expecally, this 3D network of SWNTs can enhance signal intensity dramatically in diluted solution. This system was prepared by the dipping process that makes it possible to obtain uniform distribution of network-structured CNTs among the micro Si pillar patterns. The physicochemical properties of the 3D network of SWNTs can be readily tuned by using ALD to form and engineer functional coatings on the hierarchical structures. As demonstrated in the filtering of nanoparticles, these types of functional hierarchical 3D structures offer new opportunities to develop novel microfluidic systems for a variety of biomedical and environmental applications.

3. Hierarchical Gold Micro-nanostructures based on Three-dimensional Networks of Carbon Nanotubes Fabricated by Using Electrochemical Deposition

Abstract

Three-dimensional (3D) hierarchical gold electrodes were fabricated using suspended 3D networks of carbon nanotubes (CNTs) on Si pillar templates using electrochemical deposition (ECD) in $KAu(CN)_2$ solutions. The Pt-coated networks of CNTs played an important role in providing electrical paths for ECD through discontinuous Pt layers, resulting in a vertically uniform deposition of gold on micropillars and 3D networks of CNTs connected with adjacent micropillars. The structural characteristics of the 3D hierarchical gold electrodes were superior, and their cyclic voltammograms exhibited higher peak currents and lower peak separations than those of a plain gold electrode.

Introduction

For recent years, gold has been investigated as a working electrode in biosensor applications such as DNA hybridization, protein detection, and glucose oxidase. The needs for better performance have driven a number of researchers to explore advanced gold electrodes such as porous, self-assembly monolayered, nanoparticle-modified or carbon nanotube (CNT)-modified gold electrodes. In accordance with these research efforts, the fabrication of gold electrodes with a three-dimensional (3D) structure can be a worthy endeavor to provide increased surface area and a hierarchical structure, which improve the signal intensity and the response time of biochips, depending on the dimensions and the spatial structure of both the biomaterials and the gold electrodes. Some groups have successfully fabricated 3D nanoscale gold structures by means of inverse-opal and electrochemical deposition. Recently, 3D micropillar structures of gold have been investigated to improve the detection limit in electrochemical biosensing. The detection current of biosensors is expected to be additionally enhanced by the introduction of nanowires to micropillar structures. One of the favorable approaches to realize a novel structure of gold electrodes is to deposit gold on 3D hierarchical structures by using a combination of Si micropillars with CNTs networks. In this paper, we report that a novel 3D gold electrode was successfully fabricated using 3D networks of CNTs on Si micropillars as templates by using an electrochemical deposition (ECD) method. The role of CNTs networks in ECD and the properties of the 3D hierarchical gold electrodes were investigated.

Experiment

Si pillar structures of 1 μm in diameter as templates were fabricated on highly N-type doped Si (100) wafers (LG Siltron) by the methods of anisotropic deep etching of silicon (Versaline, Oerikon). Synthesis of 3D networks of CNTs directly onto 1, 3 and 5 μm heights pillar substrates was carried out by low pressure thermal CVD method after dipping in a Fe-Mo bimetallic catalyst solution. Detail experimental procedures are described elsewhere. Pt or Cu was coated by 20 nm on CNTs-networked substrates using physical vapor deposition (PVD, E-1045, Hitachi) or atomic layer deposition (ALD, Cyclic 4000, Genitech), respectively.

A potentiostat system (WPG100, WonaTech) was employed to deposit gold on CNTs-networked pillar templates in 0.2 M $KAu(CN)_2$ (Sigma-Aldrich) solution (pH 4.0) of 30 mL by means of pulsed DC plating. A platinum wire (Sigma-Aldrich) was coiled for a counter electrode and Ag/AgCl electrode (MF-2052 RE-5B, BASi) was used as a reference electrode. In case of the substrates for cyclic voltammetry (CV), pulsed bias of ECD was applied at -1.2 V during 90, 120 and 150 sec for 1, 3 and 5 μm pillar substrates respectively. Extended biasing time was needed with increased pillar height to accomplish the corresponding deposited gold thickness of 50-70 nm. All samples were immersed in deionized water and then in ethyl alcohol for 5 min without agitation, respectively. A 100 nm thick gold-coated plane Si wafer by PVD (99.99%, Sigma-Aldrich) was chosen for commercial untreated gold electrode as a reference.

3D gold electrodes were characterized by scanning electron microscope (SEM, S-4700, Hitachi), X-ray diffractometer (XRD, ATX-G, Rigaku) and transmission electron microscope (TEM, JEM 2100F, JEOL) to understand the morphological properties and the crystallographic structures. CV of 3D gold electrodes wes conducted with a scan rate of 100 mV/sec by a CHI 660C electrochemical workstation (CH Instruments) with a conventional three-electrode electrochemical cell using the 3D gold network as a working electrode. All potentials and currents were recorded with respect to the reference electrode in N_2-saturated phosphate-buffered saline (PBS, pH 7.4) solution with 5 mM $K_4Fe(CN)_6$ (Sigma-Aldrich).

Result and Discussion

CNTs-assisted Electrochemical Deposition: 3D networks of CNTs were directly synthesized on Si micropillar templates as shown in Figure 1a. Direct gold coating on 3D networks of CNTs in ECD cell was not successful, because the networks of CNTs were disconnected by acidity (pH 4.0) or massive liquid flow during liquid processes (Figure 1b). To overcome this failure, Cu was deposited by ALD on the 3D substrate to endow the rigidness to 3D networks of CNTs against massive liquids as well as to protect suspending CNTs across Si micropillars against the acidity of the ECD cell. After Cu coating by ALD, suspending 3D networks of CNTs were preserved during liquid processes, resulting in a success of gold deposition by ECD at -2.0 V for 150 sec (Figure 1c). Nevertheless, as Cu coating by ALD process was time-consuming and expensive, Pt coating by PVD method was carried out as another methodology.

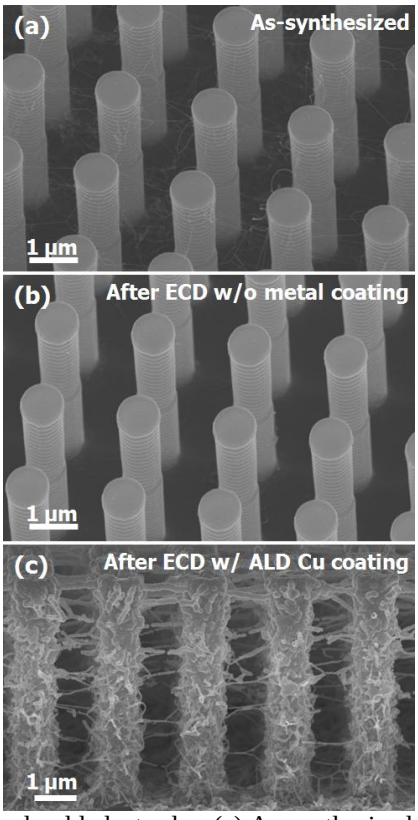

Figure 1. SEM images of 3D hierarchical gold electrodes. (a) As-synthesized, (b) after ECD without metal coating and (c) after ECD with Cu coating by ALD.

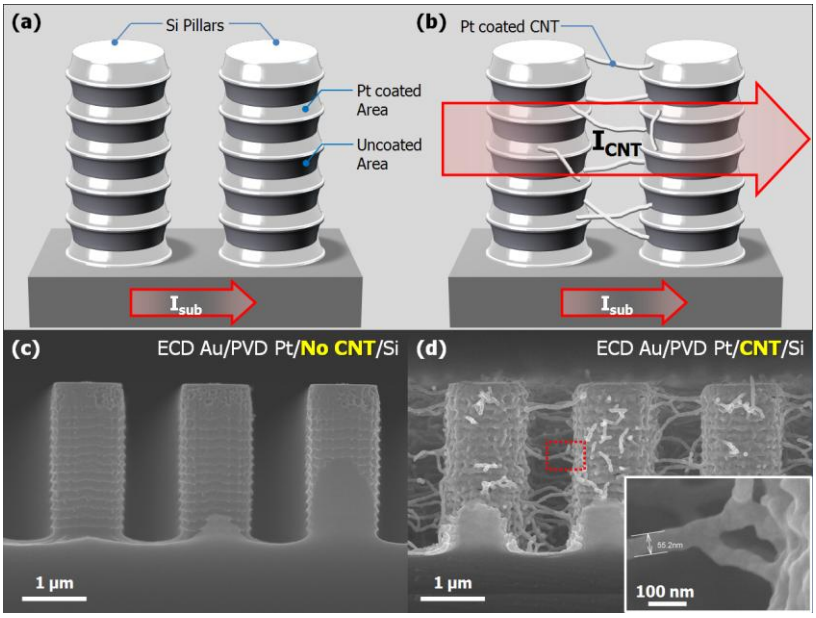

Figure 2. Schematic diagrams and SEM images of ECD of gold on Si pillar structures (a), (c) without and (b), (d) with CNTs networking, respectively. Inserted is the zoomed-in image of (d) showing nanowires of gold electrodes. Pulsed ECD was performed (c) at -1.4 V for 150 sec and (d) at -1.0 V for 240 sec, respectively.

Unlike ALD, Pt deposited by PVD is presumably anticipated to constitute innumerable flakes rather than a thin film on the lower part of each scallop of Si micropillars as illustrated in Figure

2a. Without the networks of CNTs on micropillars, deposited Pt layer on the micropillar arrays were discontinued, and then the current through a bulk substrate beneath micropillars, I_{sub}, was fully charged with the applied bias, leading to a failure of gold deposition at -1.4 V (Figure 2c). On the other hand, with 3D networks of CNTs as shown in Figure 2b, 3D electrode could secure another current path, I_{CNT}, through Pt-coated 3D networks of CNTs throughout the entire substrate area, resulting in the successful deposition of gold on the surface of 3D structures at -1.0 V, which was lower than the applied bias without 3D networks of CNTs (Figure 2d). This result proved that I_{CNT} with 3D networks of CNTs effectively promoted the nucleation rate of gold on 3D networks of CNTs and Si micropillars. Consequently, it is inferred that 3D networks of CNTs play a critical role to assist the electrochemical deposition of gold on 3D structures which were pre-modified by PVD.

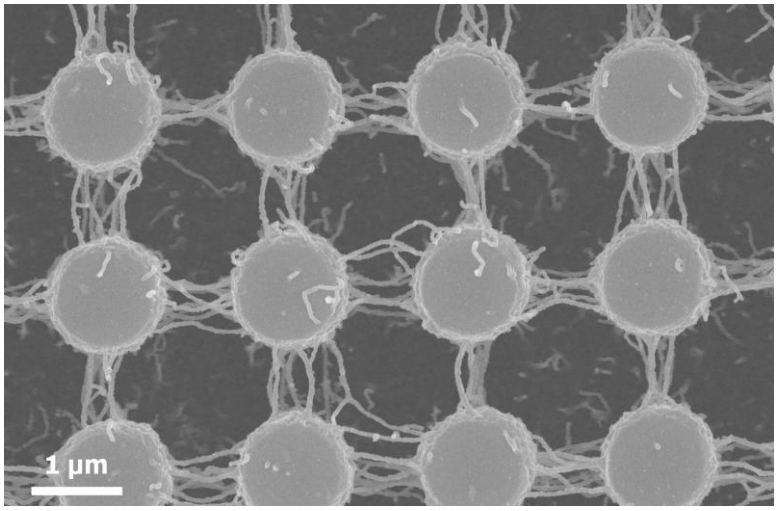

Figure 3. A top-view SEM images of hierarchical gold micro-nanostructures by ECD at pulsed -1.0 V for 180 sec.

Characterizations of 3D Hierarchical Gold Networks : Figure 3 shows a particular shape of the 3D hierarchical gold electrode deposited on micropillar templates. ECD gold was uniformly and completely coated on Si pillars of 1 μm in diameter and the networks of CNTs, which were suspending and connecting with adjacent micropillars. As a result, gold micro-arrays of 1 μm in diameter were produced with intervals of 1 μm, while gold nanowires of 50 to 60 nm in diameter were intermittently linking with two closest gold micro-arrays in vertical direction. The morphology of the 3D gold electrode was smooth, uniform and superior to the morphology of 3D gold electrode using ALD Cu in Figure 1c as well as the reported morphology of gold coating on suspended carbon nanotubes by electron-beam deposition.

From XRD data of identical sample (Figure 4a), it is obvious that 3D gold electrodes as well as a plane gold substrate by ECD had already poly crystalline structures without any further annealing treatment, and the preferred orientation was (111) plane, which is analogous to the well-known properties of gold plane substrate by PVD or thermal evaporation. Also, a cross-sectional dark field TEM image along the axis of long nanowire in Figure 4b revealed that a nanowire of gold network was composed of a large number of grains which have different brightness from each other. This result strongly indicated the poly-crystalline structure of gold nanowires deposited on suspending CNTs.

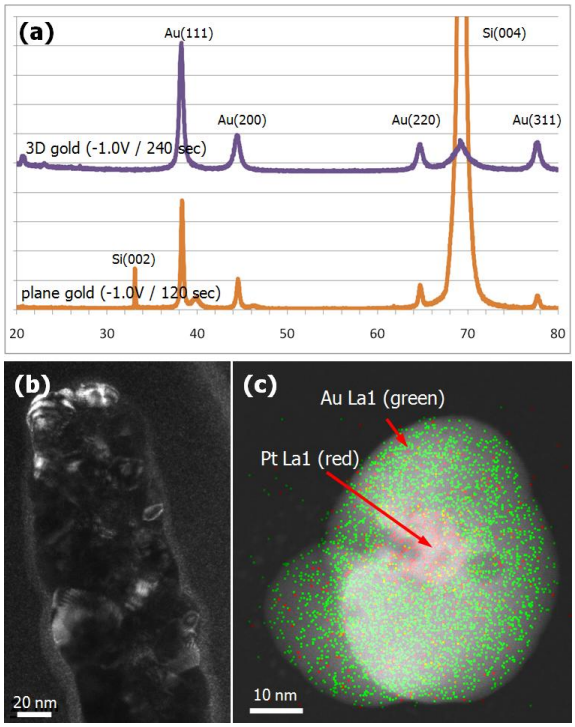

Figure 4. Structural characterizations of 3D gold electrodes. (a) XRD data, (b) cross-sectional dark field TEM image along the axis of gold nanowire and (c) cross-sectional TEM image perpendicular to the axis of gold nanowire and its energy dispersive X-ray spectrometer mapping of Pt La1 and Au La1. Pulsed ECD was performed at -1.0 V for 180 sec in case of (b) and (c).

Another cross-sectional TEM analysis was accomplished for understanding of the coating quality of gold on suspending CNTs. An area mapping of energy dispersive X-ray spectroscopy (EDX) analysis in Figure 4c represented that Pt-coated CNTs were well enveloped by gold grains in plane perpendicular to the axis of long nanowire, implying that gold nanowires were co-axially deposited by ECD even though gold electrodes were organized by nano-scale grains.

Figure 5a details cyclic voltammograms in $K_4Fe(CN)_6$ solution using both a plane gold electrode and 3D gold electrodes with 1, 3 and 5 μm heights pillars. Cyclic voltammograms of 3D gold electrodes showed wider voltammograms and higher peak currents than that of a plain gold electrode, implying the improved sensibility by the enlarged effective surface area of 3D gold electrodes. The improvement was increasingly enhanced with the height of gold micro-arrays. However, the enhancement of 3D gold electrodes was not increased as much as the increase of pillar height. Because the diffusion layers of adjacent pillars with a high pillar density overlap, only top sides of the pillars were effectively contributing to the observed current in slow scan rate of 100 mV/sec.

It is also noteworthy that the high baseline currents were observed in high positive voltage range of the curve of 3D gold electrodes, compared to the plane gold electrode. This kind of high baseline current has been reported as the capacitive charge current, which is attributed to large effective surface area. It is most likely to be an evidence corroborating the super large surface area of novel 3D gold electrodes which was not observed with 3D gold electrodes of micropillars only.

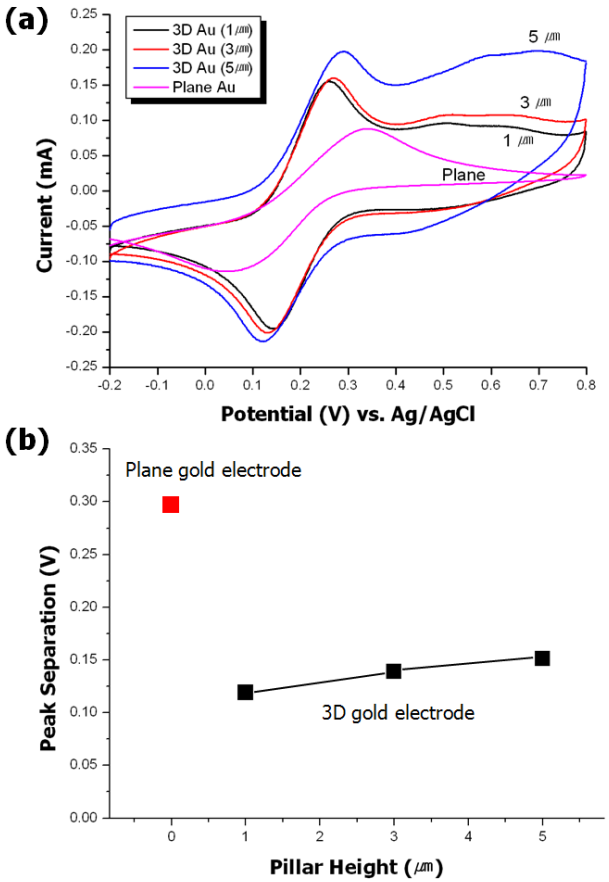

Figure 5. (a) Cyclic voltammograms and (b) the peak to peak separation of 3D gold electrodes with pillars of 1, 3 and 5 μm height and a plane gold electrode.

As plotted in Figure 5b, the separation between oxidation and reduction peaks of 3D gold electrodes were smaller than that of a plane gold electrode due to the fast mass transfer effect of micropillar structure. However, the peak separation was increased with the increasing height of gold-coated micropillars. We suggest that this outcome can result from the slower electron transfer with higher pillar heights due to the increasing resistance of the 3D gold electrode by thin thickness of gold networks.

Conclusion

3D hierarchical gold networks were electrochemically fabricated with the assistance of 3D networks of CNTs on micropillars templates. The networks of Pt coated CNTs played a critical role in successful ECD of gold to provide electrical paths through the deposited Pt layers. 3D hierarchical gold electrodes were constituted by highly ordered gold micro-arrays and gold nanowires which were co-axially coated with polycrystallinity. Compared with a plain gold electrode, cyclic voltammograms of 3D hierarchical gold electrodes represented the enhanced peak currents by increased effective surface areas as well as the small peak separations.

4. Novel 3D arrays of gold nanostructures on suspended platinum-coated carbon nanotubes as surface-enhanced Raman scattering substrates

Abstract

We report electrochemically controlled fabrications and the corresponding enhancement in Raman scattering of the three-dimensional (3D) gold arrays prepared on the template of platinum-coated carbon nanotubes (CNTs) by electrochemical deposition (ECD). The topography of deposited gold was varied from nanoparticles to nanowires by ECD conditions. The increasing surface area of 3D arrays of gold nanoparticles contributed to increase significantly the sensitivity of surface enhanced Raman scattering (SERS). For the same 3D arrays consisting of gold nanowires but with different surface roughness, much higher SERS activity was obtained when the surface of nanowires was rough.

Introduction

The fabrication of ordered gold or silver nanostructures has attracted much interest due to their broad applications in sensors based on their unique optical properties, so controlling both morphology and geometry of metal ensembles has been an important key for their applications as a substrate for surface-enhanced Raman scattering (SERS). For sensor applications especially in microfluidic devices, the spatial arrangement of metal nanostructure became one of weighty factors to increase the capture efficiency of analytes as well as SERS activity. Therefore, the three-dimensional (3D) arrays of gold or silver nanostructures are definitely advantageous SERS substrates for offering large specific surface area, spatial disposition with ease access of the analytes and a large number of hot spots within the laser-illuminated area.

We already reported the fabrication of hierarchical gold micro-nanostructure based on 3D networks of CNTs in electrochemical application-wise. In this paper, as an extension of it, we discuss electrochemically controlled fabrications and the corresponding SERS enhancements with 3D arrays of gold nanostructures on the platinum-coated CNTs templates. The correlation between the controlled morphology of gold nanostructure and the corresponding variations in Raman spectra is also provided by using rhodamine 6G (R6G) as a probe.

Experimental

Si pillar structures were first fabricated on highly N-type doped Si (100) wafers (LG Siltron Inc.) by anisotropic deep etching method. CNTs were directly synthesized onto Si pillars (3 to 8 μm height) by low pressure thermal chemical vapor deposition. Pt was coated onto the networks of CNTs with 20 nm thickness using ion sputter system (E-1045, Hitachi) to provide the electrical path for electrochemical deposition (ECD) and to secure suspended CNTs across Si

pillars during massive liquid processes, and then gold was electrochemically deposited on Pt-coated CNT templates in 0.2 M $KAu(CN)_2$ (Sigma-Aldrich) solution at pH 4.0 by applying DC pulse with a potentiostat system (WPG100, WonaTech).

After ECD, the substrates were dipped into the solution of R6G in various concentrations without stirring for 15 min, and then diluted with de-ionized water, and finally dried with high purity nitrogen gas. Raman measurements were taken with backscattering geometry on a Horiba JY LabRam HR fitted with a liquid-nitrogen cooled CCD detector. The spectra were collected under ambient conditions using the 633 nm line of a He-Ne laser (0.5mW) which was confined within 1 μm between two adjacent pillars. All gold-deposited substrates were characterized by X-ray diffractometer (XRD, ATX-G, Rigaku) after morphological analysis by scanning electron microscope (SEM, S-4700, Hitachi).

Result and Discussion

Figure 1 shows the typical 3D gold nanoparticle arrays fabricated on Pt-coated networks of CNTs by ECD with pulsed bias of -1.0 V for 120 seconds (Si pillar height = 8 μm). Gold nanoparticles with diameter of 20-30 nm were well deposited on Pt-coated networks of CNTs (Figure 1a), and formed highly-ordered 3D arrays (Figure 1b, c), and its morphology looks uniform on both CNTs and Si pillars as seen in the inserted SEM image of Figure 1 (c). From the aspect of diffusion-limited transport of analytes, 3D arrangement of gold nanoparticles is advantageous for sensor applications.

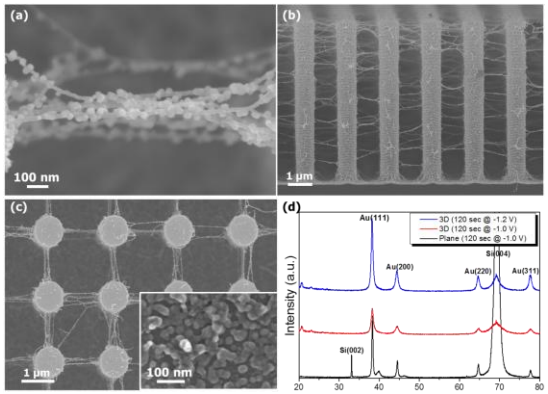

Figure 1. Morphology and crystalline structure of 3D arrays of gold nanostructures: (a), (b) cross-sectional view, (c) top view (a zoomed-in image of top area of pillar is inserted) of gold nanoparticles with 8-μm-height pillar, and (d) XRD data of two 3D and one planar gold nanostructures.

Pulsed bias condition was optimized for gold nanoparticles at -1.2 V and 120 seconds and for gold nanowires at -1.0 V and 120 seconds. Their XRD spectra show similar crystallinities to planar gold substrates (Figure 1d). Both 3D gold nanostructures and planar gold substrates are polycrystalline with the preferred orientation of (111) plane and comparable full width at half maximums.

Morphology of gold nanostructures could be controlled by the bias conditions during ECD, thus the amount of deposited gold on CNTs is estimated by the equation below.

$$\text{amount of deposited gold } (\mu\text{mol/cm}^2) = \frac{\text{biased current (C/sec)} \times \text{biased time (sec)}}{\text{area of substrate (cm}^2) \times 0.0964853365 \text{ (C/}\mu\text{mol)}}$$

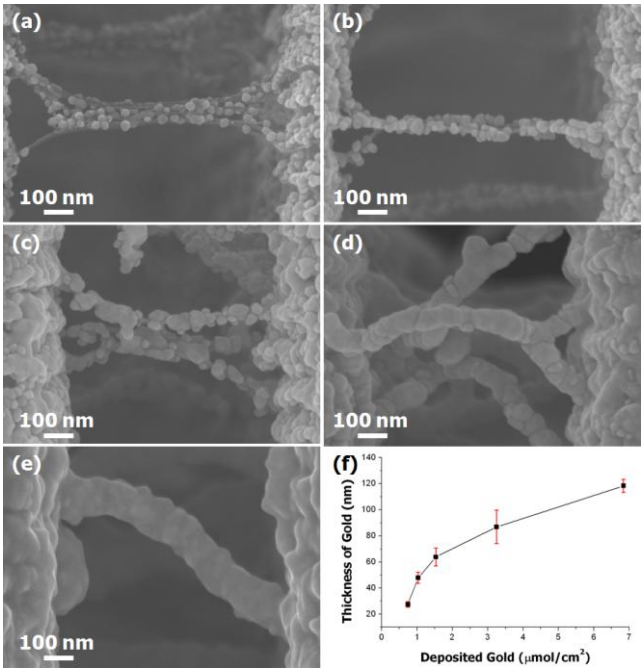

Figure 2. SEM images of the controlled morphology of gold nanostructures by varying the amount of deposited gold to (a) 0.74 μmol/cm^2, (b) 1.03 μmol/cm^2, (c) 1.53 μmol/cm^2, (d) 3.25 μmol/cm^2 and (e) 6.84 μmol/cm^2. (f) is the measured thickness of gold nanostructure with the amount of deposited gold.

Figure 2 represents the morphology control of gold nanostructures on CNTs by varying the amount of gold deposited. The calculated gold amounts are 0.74, 1.03, 1.53, 3.25 and 6.84 μmol/cm^2 for the samples in Figure 2a-e, respectively. As the amount is increased, the gold nanoparticles are merged to form smooth gold nanowires. It was expected to form tubular structures eventually because gold nuclei were templated on CNTs. The measured thickness of gold on CNTs was increased proportionally to the square root of the deposited gold amount (Figure 2f). Considering only gold deposited on single suspended CNT, this result consists well with the relationship between the tube radius (the thickness of gold) and the mass (the amount of deposited gold), supporting that the morphology of gold is successfully controlled by the amount of deposited gold.

SERS spectra obtained from 3D arrays of gold nanostructures are presented in Figure 3. Gold nanoparticles prepared with 0.74 μmol/cm^2 do not exhibit strong SERS effect because of the small surface area of gold for the adsorption of R6G molecules. Intensity increase of the peak at 1362 cm^{-1} from 0.74 to 3.25 μmol/cm^2 is likely attributed to the increase in surface area of the deposited gold. Besides the enhancement by larger surface area, there may be another enhancement by hot spots in the ensemble of gold nanoparticles. However, it was not possible to distinguish the enhancement by hot spots from that by the increasing surface area.

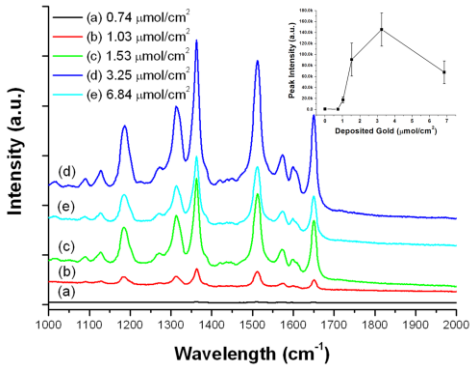

Figure 3. SERS spectra of 3D array of gold nanostructures with 3 μm-pillar heights. Each spectrum is the averaged profile of 5 measurements at the different locations. Inserted is the peak intensity at 1362 cm^{-1} in the function of deposited gold.

It is noteworthy that the peak intensity for 6.84 μmol/cm^2 is less than half of that for 3.25 μmol/cm^2 although its surface area is larger. It is inferred that there were hot spots in gold nanowires formed at 3.25 μmol/cm^2. Judging from the difference of morphology between gold nanowires of 3.25 and 6.84 μmol/cm^2, the reduced surface roughness of gold nanowires formed at 6.84μmol/cm^2 likely affects the enhancement of Raman scattering by the electromagnetic theory of SERS. Presumably hot spots were at the rough boundaries of merged gold nanoparticles, but would be disappeared at 6.84μmol/cm^2.

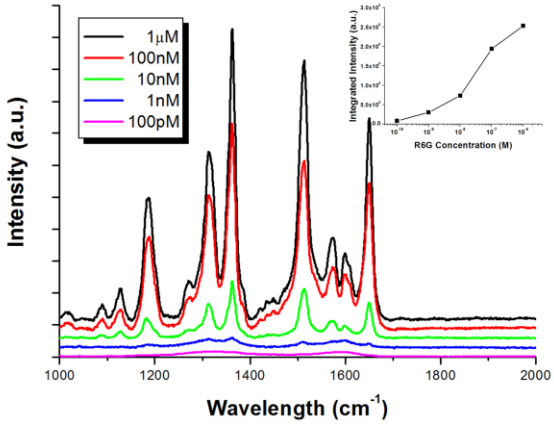

Figure 4. SERS spectra of 3D array of gold nanostructures (3.25 μmol/cm^2) at different R6G concentrations. Each spectrum is the averaged profile of 3 measurements at the different locations. Inserted is the peak intensity at 1362 cm^{-1} versus R6G concentrations.

Figure 4 shows the SERS spectra of 3D gold substrates (3.25 μmol/cm^2) with R6G concentrations varied from 1 μM to 100 pM. The peaks for R6G molecules were decreased with the R6G concentration down to 1 nM, and disappeared completely at 100 pM. Thus, the detection limit achieved from this approach is 1 nM.

The SERS surface enhancement factor (EF) is calculated for R6G on the Au nanostructured samples (Figure 2d) according to the equation $EF=(I_{surf}/N_{surf})/(I_{Raman}/N_{Raman})$. In this expression, I_{surf} and I_{Raman} stand for the integrated intensities for the 1362 cm^{-1} peak of the R6G adsorbed on the Au surface and

R6G on the bare Si surface, respectively; whereas N_{surf} and N_{Raman} represent the corresponding number of R6G molecules excited by the laser beam. 20 μl of 1 μM and 1 mM R6G methanol solutions were drop-casted on 3D array of gold substrate and the bare Si wafer which top-view areas are 0.85 cm^2, respectively. The effective occupied area of single R6G molecule onto 3D array of gold substrate and the bare Si substrate was about 7000 and 7 nm^2, respectively. Assuming the projected area by laser at 3D gold SERS substrate is similar to that of the bare Si substrate, the maximum EF of 1.4×10^9 is achieved.

Conclusion

The 3D gold arrays for SERS-active substrate were electrochemically fabricated using the Pt-coated networks of CNTs as a template. The crystallinity of gold nanostructures was polycrystalline with the preferred orientation of (111) plane. The morphology of deposited gold was successfully controlled from nanoparticles to nanowires by varying the amount of gold. The intensity of SERS spectra using R6G were varied depending on the surface area and the roughness of gold. The peak intensity of 1362 cm^{-1} had a maximum within the range of 0.74 and 6.84μmol/cm^2 by the competing effects on the enhancement between the increased surface area and the reduced surface roughness of gold.

List of Publications and Significant Collaborations that resulted from your AOARD supported project

a) papers published in peer-reviewed journals

(1) Jeongeun Seo , Tae Jae Lee , Seungbin Ko , Haegu Yeo , Suhawn Kim , Taeyong Noh ,Simon Song , Myung M. Sung , Haiwon Lee., Hierarchical and Multifunctional Three-dimensional Network of Carbon Nanotubes for Microfl uidic Applications. *Advanced Materials* **2012,** *24* 1975. (16. Mar.2012)

(2) Moon-Keun Lee, Seok Jin Cho, Youngdeok Jo and Haiwon Lee., Hierarchical Gold Micro-nanostructures based on Three-dimensional Networks of Carbon Nanotubes Fabricated by Using Electrochemical Deposition. *Journal of the Korean Physical Society* **2012,** *60,* 1135. (14. Feb. 2012)

(3) Moon-Keun Lee, Jeongeun Seo, Seok Jin Cho. Yongdeok Jo, Seonae Kim, Youngjong Kang, Haiwon Lee,. Novel 3D arrays of gold nanostructures on suspended platinum-coated carbon nanotubes as surface-enhanced Raman scattering substrates. *Materials Letters,* **2012,** *81***, 9.** (3. May. 2012)

b) papers published in peer-reviewed conference proceedings

c) papers published in non-peer-reviewed journals and conference proceedings

d) conference presentations without papers

(1) Jeongeun Seo, Hyunsook Kim, Haegu Yeo, Seok Jin Cho, Yongdeok Jo, Haiwon Lee,. Effective Filtration System using Three-Dimensional Carbon Nanotube Networks Template as Microfluidic chip, **NANOMED 2011** (9. Nov. 2011)

(2) Jeongeun Seo, Hyunsook Kim, Haegu Yeo, Seok Jin Cho, Yongdeok Jo, Haiwon Lee,. Single-walled Carbon Nanotube Growth on Fe/Mo-sprayed Si Substrate. **NMDC 2011** (18. Nov. 2011)

(3) Seok Jin Cho, Jeongeun Seo, Hyunsook Kim, Haegu Yeo, Yongdeok Jo, Moon-Keun Lee, Haiwon Lee,. Electrochemical deposition of gold substrate on three-dimensional structure. **Autumn KCS 2011** (30. Sep. 2011)

(4) Yongdeok Jo, Jeongeun Seo, Hyunsook Kim, Haegu Yeo, Seok Jin Cho, Moon-Keun Lee, Haiwon Lee,. Fabrication of carbon nanotube on the catalyst patterned substrate using photolithography. **Autumn KCS 2011** (30. Sep. 2011)

(5) Jeongeun Seo, Haegu Yeo, Teayoung Noh, Haiwon Lee,. Efficient Synthesis of Single-walled Carbon Nanotubes using Spray Method. **NANO KOREA 2011** (24. Aug. 2011)

(6) Jeongeun Seo, Seojin Cho, Yong-deok Jo, Seonae Kim, Haiwon Lee,. Hierarchical and Multifunctional Three-Dimensional Network of Carbon Nanotubes for Microfluidic Applications. **US-KOREA JSNT Workshop 2012** (1. May. 2012)

(7) Haiwon Lee,. Hierarchical and Muntifunctional Three-dimensional Network of Carbon Nanotubes for Microfluidic and Strain Sensor Applications. **US-KOREA JSNT Workshop 2012** (1. May. 2012)

e) manuscripts submitted but not yet published

f) provide a list any interactions with inadustry or with Air Force Research Laboratory scientists or significant collaborations that resulted from this work.